FACTA UNIVERSITATIS
Series: **Physics, Chemistry and Technology** Vol. 7, N° 1, 2009, pp. 33 - 44
DOI: 10.2298/FUPCT0901033R

APPLICATION OF THE LEVEL SET METHOD ON THE NON-CONVEX HAMILTONIANS

UDC 519.876.5

B. Radjenović[1], M. Radmilović-Radjenović[1], M. Mitrić[2]

[1]Institute of Physics, Pregrevica 118, Belgrade, Serbia
[2]Vinča Institute of Nuclear Sciences, P. O. Box 522, 11001 Belgrade, Serbia

Abstract. *Application of the level set method extended for the case of non-convex Hamiltonians is illustrated by the three dimensional (3D) simulation results of the profile evolution during anisotropic wet etching of silicon. Etching rate function is modeled on the basis of the silicon symmetry properties, by means of the interpolation technique using experimentally obtained values of the principal [100], [110], [111], and high index [311] directions in KOH solutions. The resulting level set equations are solved using an open source implementation of the sparse field method.*

Key words: *Etching, level set, profile evolution, simulation*

INTRODUCTION

Micro and Nano Electro Mechanical systems (M(N)EMS) represent a rapidly expanding field of semiconductor fabrication technologies for producing micro and nano scale mechanical, electric, optical, fluidic, and other devices [1]. In an ideal M(N)EMS design environment, refined control of etched profiles is one of the most important tasks of M(N)EMS manufacturing process. In spite of its wide use, the simulation of etching for M(N)EMS applications has been so far a partial success only, although a great number of commercial and academic research tools dedicated to this problem are developed.

Actually, two types of simulations exist [2]: the first category comprises simulators describing etching process on the atomistic level, usually including the description of etched surface morphologies. The second type deals with the prediction of the etching profile evolution in engineering applications, typically including the combination of etching with other MEMS manufacturing techniques. The so called atomistic simulators based on Cellular Automata and Monte Carlo methods [2-7] belong to the former group. In this methods, a silicon substrate is represented by a large number of cells that reside in a crystalline lattice. During the etching process, the state of each individual cell, i.e. whether it is removed from or remains within the lattice, is determined by the strength of chemical bonds and link status of its lattice neighbors. Also, the step-flow aspect [8] of

Received November 29, 2009

wet etching process fits well into Cellular Automata method [7]. Until now, the most common type the of the engineering simulators are so called geometrical simulators [9].

The level set method for evolving interfaces [10] belongs to the geometric type of methods, and it is specially designed for profiles which can develop sharp corners, change of topology and undergo orders of magnitude changes in speed. It is based on Hamilton–Jacobi type equation for the level set function using techniques developed for solving hyperbolic partial differential equations. This method is free from any implicit assumptions about the nature of the processes that force interface evolution, and the whole physics and chemistry of them are contained in just one parameter - normal component of the surface velocity. During the last years several variants of the level set methods have been developed with application to micro fabrication problems [11,12]. In this study we present an anisotropic etching simulator based on the sparse field method for solving the level set equations. The sparse-field method itself, developed by Whitaker [13], and broadly used in image processing community, is an alternative to the usual combination of narrow band and fast marching procedures for the computationally effective solving of the level set equations [14,15]. Our primary goal is to develop an accurate, stable and efficient 3D code for tracking of the etching profile evolution that includes different physical effects such as anisotropy and material-dependent propagation rates, yet being computationally effective to run on desktop PCs.

The paper is organized as follows: in section II some aspect of the silicon wet etching process are discussed. After that, the relations describing the angular dependence of the etching rates, based on an interpolation procedure and silicon crystal symmetry properties, are derived. In section III the necessary details for the implementation of the sparse field method for solving the level set equations in the case of etching rates defined in section II, are described. Section IV contains detailed analysis of the obtained simulation results for some interesting initial 3D shapes (cube and sphere).

ANISOTROPIC WET ETCHING OF SILICON. ANGULAR DEPENDENCE OF THE ETCHING RATE

Although silicon etching techniques are currently undergoing a revolution driven by the incorporation of plasma etching process, anisotropic wet chemical etching is still the most widely used processing technique in silicon technology [1].

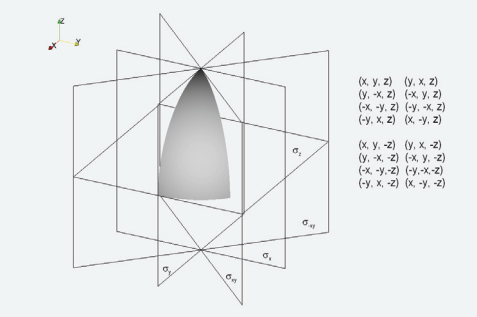

Fig. 1. The angular section defined by the planes ($0 \le N_x$; $0 \le N_y \le N_x$; $0 \le N_z$) where the interpolation is performed. The symmetry elements and the symmetry operations are denoted.

Not only the cost of wet etching systems is much lower than that of plasma types, but also certain features can only be realized using anisotropic wet etching. Very complicated 3D structures can be formed by this technique; it enables controlled undercutting of suspended structures, not possible by other microfabrication techniques. It is also referred to as "bulk micromachining", since in this technology the body of the silicon wafer is etched away.

The anisotropy of the etching process is actually the orientation dependence of the etch rate. Regardless of the great amount of work done in this field, there is no generally accepted single theory for a mechanism that explains the great anisotropy in silicon wet etching. It is accepted [6] that the origin of this macroscopic anisotropy in the etching process lies in the crystal site-specificity of the etch rates at the atomistic level.

As stated earlier, in order to simulate the time evolution of 3D etching profiles it is essential that exact etch rates in all directions are known. The etching rates for only a few principal axes are known, but they can be used to determine rate value in an arbitrary direction by an interpolation procedure. The problem of etching rate interpolation is equivalent to function interpolation over a sphere in 3D. For accuracy, the etching rate model must interpolate through the given etching rates and directions while maintaining its continuity, since possible requirement that the first derivative must be continuous also, is too high, as empirical studies have shown cusps in etching rate diagrams.

Here we shall use etching rate model developed by Hubbard [9], that satisfies these conditions. Of course, this is not the only possibility; the problem of finding the optimal interpolation method is out of scope of this paper. It is supposed that x, y and z axes are aligned with [100], [010] and [001] crystal directions, respectively. The point group of silicon's symmetry *m3m* (subgroup of Fd3m space group) contains 48 elements. Since it is not easy to assemble angular section using three principal directions with which the whole space can be covered by the symmetry operations, only 16 out of 48 symmetry elements can be used for that purpose. As a result, it is necessary to look only at 1/16th of the all full angular extent ($0 \le \theta \le 90°$; $0 \le \phi \le 45°$), or at the wedge defined by the planes ($0 \le N_x$; $0 \le N_y \le N_x$; $0 \le N_z$), as it is shown in Fig. 1. The angular section, shown in gray in Fig. 1, is the region where the etching rate should be interpolated. The simplest method is to use only the experimental rate values for the principal directions [100], [110] and [111], since in three dimension three independent vectors are needed to define a basis. In that case, the interpolation region is actually the union of three sections defined by the principal vectors A[100, 111, 110], B[100, 111, 101] and C[001, 111, 101] (see Fig. 2a).

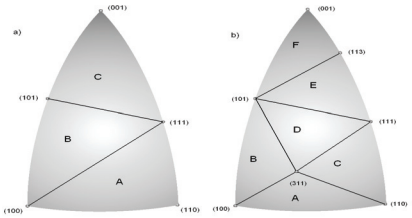

Fig. 2. The a) three- and b) four-parameters inetrpolation regions.

Following the procedure described in Ref. [9], the etching rate R in an arbitrary direction $\mathbf{N}(N_x, N_y, N_z)$ is then given by the interpolation relation:

$$R(\mathbf{N}) = \begin{cases} [R_{100}(N_x - N_y) + R_{110}(N_y - N_z) + R_{111}N_z]/N_x; & \mathbf{N} \in A \\ [R_{100}(N_x - N_z) + R_{110}(N_z - N_y) + R_{111}N_y]/N_x; & \mathbf{N} \in B \\ [R_{100}(N_z - N_x) + R_{110}(N_x - N_y) + R_{111}N_y]/N_z; & \mathbf{N} \in C \end{cases}, \quad (1)$$

where R_{hkl} is etching rate in [hkl] direction. Changing to the spherical coordinates:

$$N_x = \sin\theta\cos\phi; \quad N_y = \sin\theta\sin\phi; \quad N_z = \cos\theta, \quad (2)$$

it is straightforward to obtain the following three-parameter (R_{100}, R_{110}, and R_{111}) etching rate angular dependence:

$$R(\theta,\phi) = \begin{cases} R_{100} - (R_{110} - R_{111})\cot\theta/\cos\phi + (R_{110} - R_{100})\tan\phi; & (\theta,\phi) \in A \\ R_{100} + (R_{110} - R_{100})\cot\theta/\cos\phi + (R_{111} - R_{110})\tan\phi; & (\theta,\phi) \in B \\ R_{100} + [(R_{110} - R_{100})\cos\phi + (R_{110} - R_{100})\sin\phi]\tan\theta; & (\theta,\phi) \in C \end{cases}. \quad (3)$$

In Fig. 3 the resulting etching rate is shown in the full angular extent. The presence of cusps in the etching rates implies the existence of facets in the etching profiles.

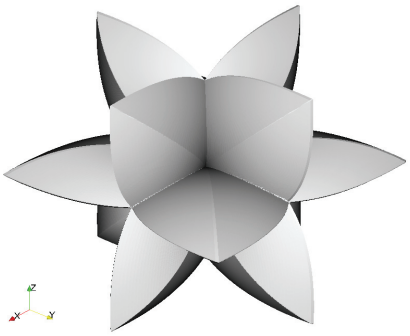

Fig. 3. The angular dependence of the etching rate calculated using three-parameter interpolation formula (3), for R_{111} = 0.005 μm/min, R_{100} = 0.797 μm/min, R_{110} = 1.455 μm/min.

Better interpolation results can be obtained if additional experimentally obtained rates are included. For example, if include the next most important (high index) planes {311}, the interpolation region will consist of six sections: A[100, 311, 110], B[100, 101, 311], C[311, 111, 110], D[311, 101, 111], E[101, 113, 111] and F[101, 001, 113], as it is depicted in Fig.2b. Then, the etching rate R in an arbitrary direction $\mathbf{N}(N_x, N_y, N_z)$ will be given by the relation:

$$R(\mathbf{N}) = \begin{cases} [R_{100}(N_x - N_y - 2N_z) + R_{110}(N_y - N_z) + 3R_{311}N_z]/N_x; & \mathbf{N} \in A \\ [R_{100}(N_x - 2N_y - N_z) + R_{110}(N_z - N_y) + 3R_{311}N_y]/N_x; & \mathbf{N} \in B \\ \{R_{111}[(N_y - N_x)/2 + N_z] + R_{110}(N_y - N_z) + 3R_{311}(N_x - N_y)/2\}/N_x; & \mathbf{N} \in C \\ [R_{111}(2N_y - N_x + N_z)/2 + R_{110}(N_z - N_y) + 3R_{311}(N_x - N_z)/2]/N_x; & \mathbf{N} \in D \\ [R_{111}(N_x + 2N_y - N_z)/2 + R_{110}(N_x - N_y) + 3R_{311}(N_z - N_x)/2]/N_z; & \mathbf{N} \in E \\ [R_{100}(N_z - N_x - 2N_y) + R_{110}(N_x - N_y) + 3R_{311}N_y]/N_z; & \mathbf{N} \in F \end{cases}, \quad (4)$$

and corresponding angular dependence becomes:

$$R(\theta,\phi) = \begin{cases} R_{100} - (2R_{100} + R_{110} - 3R_{311})\cot\theta/\cos\phi + (R_{110} - R_{100})\tan\phi; & (\theta,\phi) \in A \\ R_{100} + (R_{110} - R_{100})\cot\theta/\cos\phi - (2R_{100} + R_{110} - 3R_{311})\tan\phi; & (\theta,\phi) \in B \\ (3R_{311} - R_{111})/2 + (R_{111} - R_{110})\cot\theta/\cos\phi + [R_{110} + (R_{111} - 3R_{311})/2]\tan\phi; & (\theta,\phi) \in C \\ [3R_{311} - R_{111} + (2R_{110} + R_{111} - 3R_{311})\cot\theta/\cos\phi + 2(R_{111} - R_{110})\tan\phi]/2; & (\theta,\phi) \in D \\ \{3R_{311} - R_{111} + [(2R_{110} + R_{111} - 3R_{311})\cos\phi + (R_{111} - R_{110})\sin\phi]\tan\theta\}/2; & (\theta,\phi) \in E \\ R_{100} - [(R_{100} - R_{110})\cos\phi + (2R_{100} + R_{110} - 3R_{311})\sin\phi]\tan\theta; & (\theta,\phi) \in F \end{cases}. \quad (5)$$

Fig. 4 shows the four-parameter angular dependence for the values of parameters (R_{100}, R_{110}, R_{111}, and R_{311}) used in subsequent simulation examples. There is no any principal difficulty in including other known high index etching rates, only the resulting analytical expression will become more complicated.

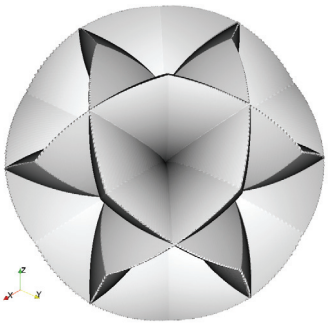

Fig. 4. The angular dependence of the etching rate calculated using four-parameter interpolation formula (5), for R_{111} = 0.005 μm/min, R_{100} = 0.797 μm/min, R_{110} = 1.455 μm/min and R_{311} = 1.436 μm/min.

It is important to remember that all physical aspects of the etching process are contained in these angular dependences, and that they determine time evolution of the feature profile completely, appearance and disapearrance of particular planes and the final profile. For different values of the parameters these shapes look different. Inclusion of additional planes will also change the shape of angular dependences.

LEVEL SET METHOD FOR NON-CONVEX HAMILTONIANS

Level set method, introduced by Osher and Sethian [10], is a powerful technique for analyzing and computing moving fronts in a variety of different settings. The level sets are used in image processing, computer vision, computational fluid dynamics, material science, and many other fields. Detailed exposition of the theoretical and numerical aspects of the method, and applications to different areas can be found in books [14,15], and recent review articles [16,17]. The basic idea behind the level set method is to represent the surface in question at a certain time t as the zero level set (with respect to the space variables) of a certain function φ (t, $\mathbf{x}$), the so called level set function. The level set equation:

$$\frac{\partial \varphi}{\partial t} + R(t, \mathbf{x}) \left| \nabla \varphi \right| = 0 , \tag{6}$$

with the unknown function φ (t, $\mathbf{x}$), where $\varphi(0, \mathbf{x}) = 0$ determines the initial surface, can be rewritten in Hamilton–Jacobi form:

$$\frac{\partial \varphi}{\partial t} + H(\nabla \varphi(t, \mathbf{x})) = 0, \tag{7}$$

where Hamiltonian is given by $H = R\ (t, \mathbf{x})|\nabla \varphi(t, \mathbf{x})|$ (in this context the term "Hamiltonian" denotes a Hamiltonian function, not an operator). A detailed exposition about the Hamilton–Jacobi equation, the existence and uniqueness of its solution (especially about its viscosity solutions), can be found in Ref. [18]. We say that such a Hamiltonian is convex (in $\Re^n$) if the following condition is fulfilled:

$$\frac{\partial^2 H}{\partial \varphi_{x_i} \partial \varphi_{x_j}} \geq 0 \tag{8}$$

where φ_{x_i} is a partial derivative of $\varphi(t, \mathbf{x})$ with respect of x_i . If the surface velocity R (t, $\mathbf{x}$) does not depend on the level set function $\varphi(t, \mathbf{x})$ itself, this condition is usually satisfied. In that case, we can say that the problem is of free boundary type. In that case the spatial derivatives of φ can be approximated using the Engquist-Osher upwind finite difference scheme, or by ENO (higher-order essentially non-oscillatory) and WENO (weighted essentially non-oscillatory) discretization schemes, that requires the values of this function at the all grid points considered. The resulting semi-discrete equations can be solved using explicit Euler method, or more precisely by TVD (total-variation diminishing) Runge-Kutta time integration procedure (see Refs. [14] and [15] for the details).

Several approaches for solving level set equations exist which increase accuracy while decreasing computational effort. They are all based on using some sort of adaptive schemes. The most important are narrow band level set method, widely used in etching process modeling tools, and recently developed sparse-field method [13], implemented in medical image processing ITK library [19]. The sparse-field method use an approximation to the distance function that makes it feasible to recompute the neighborhood of the zero level set at each time step. It computes updates on a band of grid points that is only one point wide. The width of the neighborhood is such that derivatives for the next time step can be calculated. This approach has several advantages. The algorithm does pre-

cisely the number of calculation needed to compute the next position of the zero level set surface. The number of points being computed is so small that it is feasible to use a linked-list to keep a track of them, so at each iteration only those points are visited whose values control the position of the zero level set surface. As a result, the number of computations increases with the size of the surface, rather than with the resolution of the grid.

The non-convex Hamiltonians are characteristic for anisotropic etching and deposition simulations [12].The upwind finite difference scheme cannot be used in the case of non-convex Hamiltonians. The simplest scheme that can be applied in these cases is the Lax–Friedrichs, one which relies on the central difference approximation to the numerical flux function, and preserves monotonicity through a second-order linear smoothing term [15]:

$$\varphi_{ijk}^{n+1} = \varphi_{ijk}^{n} - \Delta t[H\left(\frac{D_{ijk}^{-x} + D_{ijk}^{+x}}{2}, \frac{D_{ijk}^{-y} + D_{ijk}^{+y}}{2}, \frac{D_{ijk}^{-z} + D_{ijk}^{+z}}{2}\right) - \frac{1}{2}\alpha_x (D_{ijk}^{+x} - D_{ijk}^{-x}) - \frac{1}{2}\alpha_y (D_{ijk}^{+y} - D_{ijk}^{-y}) - \frac{1}{2}\alpha_z (D_{ijk}^{+z} - D_{ijk}^{-z})], \tag{9}$$

where $D_{ijk}^{+x(y,z)}$ and $D_{ijk}^{-x(y,z)}$ are usual forward and backward differences:

$$\begin{aligned} D_{ijk}^{+x} &= \frac{\varphi_{i+1,j,k}^{n} - \varphi_{i,j,k}^{n}}{\Delta x}, \quad D_{ijk}^{-x} = \frac{\varphi_{i,j,k}^{n} - \varphi_{i-1,j,k}^{n}}{\Delta x} \\ D_{ijk}^{+y} &= \frac{\varphi_{i,j+1,k}^{n} - \varphi_{i,j,k}^{n}}{\Delta y}, \quad D_{ijk}^{-y} = \frac{\varphi_{i,j,k}^{n} - \varphi_{i,j-1,k}^{n}}{\Delta y}, \\ D_{ijk}^{+z} &= \frac{\varphi_{i,j,k}^{n} - \varphi_{i,j,k+1}^{n}}{\Delta z}, \quad D_{ijk}^{-z} = \frac{\varphi_{i,j,k}^{n} - \varphi_{i,j,k-1}^{n}}{\Delta z} \end{aligned} \tag{10}$$

and $\alpha_x(\alpha_y, \alpha_z)$ is a bound on the partial derivative of the Hamiltonian with respect to the first (second, third) argument:

$$\alpha_x = \max\left|\frac{\partial H}{\partial \varphi_x}\right|, \quad \alpha_y = \max\left|\frac{\partial H}{\partial \varphi_y}\right|, \quad \alpha_z = \max\left|\frac{\partial H}{\partial \varphi_z}\right|. \tag{11}$$

It is essential to express the etching rates in terms of the level set function itself in order to obtain level set equation in Hamilton-Jacobi form. To accomplish this goal, we start from the facts that the unit vector normal to the zero level set is given by $\mathbf{N} = \nabla\varphi / |\nabla\varphi|$, and that the angles θ and ϕ are connected to the level set function by the $\sin\theta = \sqrt{1 - \varphi_z^2 / |\nabla\varphi|^2}$ and $tg\phi = \varphi_y / |\nabla\varphi|$. In this way the rate R can be expressed in terms of the geometrical properties of the level set function itself, and the Hamiltonian becomes:

$$H(\nabla\varphi)=\begin{cases}|\nabla\varphi|[R_{100}\varphi_x+(R_{110}-R_{100})\varphi_y+(R_{111}-R_{110})\varphi_z]/\varphi_x; & \nabla\varphi\in A\\ |\nabla\varphi|[R_{100}\varphi_x+(R_{111}-R_{110})\varphi_y+(R_{100}+R_{110})\varphi_z]/\varphi_x; & \nabla\varphi\in B\\ |\nabla\varphi|[(R_{110}-R_{100})\varphi_x+(R_{111}-R_{110})\varphi_y+R_{100}\varphi_z]/\varphi_z; & \nabla\varphi\in C\end{cases}, \tag{12}$$

for the simple etching rate angular dependence given by the relation (3). In order to implement Lax–Friedrichs scheme it is necessary to find first derivatives appearing in (11). After some straightforward algebraic manipulations the following relations can be obtained:

$$\frac{\partial H}{\partial\varphi_x}=\begin{cases}\{R_{100}(\varphi_x^3+\varphi_y^3+\varphi_y\varphi_z^2)-[R_{110}(\varphi_y-\varphi_z)+R_{111}\varphi_z](\varphi_y^2+\varphi_z^2)\}/(\varphi_x^2|\nabla\varphi|); & \nabla\varphi\in A\\ \{R_{100}(\varphi_x^3+\varphi_y^2\varphi_z+\varphi_z^3)-[R_{110}(\varphi_z-\varphi_y)+R_{111}\varphi_y](\varphi_y^2+\varphi_z^2)\}/(\varphi_x^2|\nabla\varphi|); & \nabla\varphi\in B\\ \{R_{111}\varphi_x\varphi_y+(R_{110}-R_{100})(|\nabla\varphi|^2+\varphi_x^2)+(R_{110}\varphi_y-R_{100}\varphi_z)\varphi_x\}/(\varphi_z|\nabla\varphi|); & \nabla\varphi\in C\end{cases}, \tag{13}$$

$$\frac{\partial H}{\partial\varphi_y}=\begin{cases}[R_{111}\varphi_y\varphi_z+(R_{110}-R_{100})(|\nabla\varphi|^2+\varphi_y^2)-(R_{100}\varphi_x+R_{110}\varphi_z)\varphi_y]/(\varphi_x|\nabla\varphi|); & \nabla\varphi\in A\\ [R_{100}\varphi_y(\varphi_x-\varphi_z)+(R_{111}-R_{110})(|\nabla\varphi|^2+\varphi_y^2)+R_{110}\varphi_y\varphi_z]/(\varphi_x|\nabla\varphi|); & \nabla\varphi\in B\\ [R_{100}\varphi_y(\varphi_z-\varphi_x)+(R_{111}-R_{110})(|\nabla\varphi|^2+\varphi_y^2)+R_{110}\varphi_y\varphi_x]/(\varphi_z|\nabla\varphi|); & \nabla\varphi\in C\end{cases}, \tag{14}$$

$$\frac{\partial H}{\partial\varphi_z}=\begin{cases}\{(R_{111}-R_{110})(\varphi_x^2+\varphi_y^2)+[R_{100}(\varphi_x-\varphi_y)+R_{110}\varphi_y]\varphi_z-2(R_{110}-R_{111})\varphi_z^2\}/(\varphi_x|\nabla\varphi|); & \nabla\varphi\in A\\ \{(R_{110}-R_{100})(\varphi_x^2+\varphi_y^2)+[R_{100}\varphi_x+(R_{111}-R_{110})\varphi_y]\varphi_z+2(R_{110}-R_{100})\varphi_z^2\}/(\varphi_x|\nabla\varphi|); & \nabla\varphi\in B\\ \{[(R_{100}-R_{110})\varphi_x+(R_{110}-R_{111})\varphi_y](\varphi_x^2+\varphi_y^2)+R_{100}\varphi_z^3\}/(\varphi_z^2|\nabla\varphi|); & \nabla\varphi\in C\end{cases}. \tag{15}$$

If the high index planes {311} are included, the expressions become more complicated because the interpolation region is then divided in six sub-regions. Since one of the goals of this study is to investigate the influence of these planes on the final outcomes, we shall write them explicitly. The Hamiltonian corresponding to the relation (5) has the form:

$$H(\nabla\varphi)=\begin{cases}|\nabla\varphi|[R_{100}\varphi_x+(R_{110}-R_{100})\varphi_y+(3R_{311}-R_{100}-R_{110})\varphi_z]/\varphi_x; & \nabla\varphi\in A\\ |\nabla\varphi|[R_{100}\varphi_x+(3R_{311}-2R_{100}-R_{110})\varphi_y+(R_{110}-R_{100})\varphi_z]/\varphi_x; & \nabla\varphi\in B\\ |\nabla\varphi|\{(3R_{311}-R_{111})\varphi_x/2+(R_{111}/2+R_{110})\varphi_y-(R_{110}+3R_{311}/2)\varphi_z\}/\varphi_x; & \nabla\varphi\in C\\ |\nabla\varphi|[(3R_{311}-R_{111})\varphi_x/2+(R_{111}-R_{110})\varphi_y+(R_{110}+R_{111}/2-3R_{311}/2)\varphi_z]/\varphi_x; & \nabla\varphi\in D\\ |\nabla\varphi|[(3R_{311}/2+R_{110}+R_{111}/2)\varphi_x+(R_{111}-R_{110})\varphi_y+(3R_{311}-R_{111})\varphi_z/2]/\varphi_z; & \nabla\varphi\in E\\ |\nabla\varphi|[(R_{110}-R_{100})\varphi_x+(3R_{311}-2R_{100}-R_{110})\varphi_y+R_{100}\varphi_z]/\varphi_z; & \nabla\varphi\in F\end{cases}, \tag{16}$$

The first and second derivatives of the Hamiltonian appearing in (12) and (16), needed for checking their convexity condition (8), are too cumbersome to be stated here. Actually, it is not necessary as it is obvious, from the Figs. 2 and 3, that the etching rates (and corresponding Hamiltonians) are non-convex functions. It means that it is convenient to implement already mentioned procedure [20] in order to solve numerically initial value problem (7).

SIMULATION RESULTS

Potassium hydroxide (KOH) is the most common and the most important chemical etchant, because of its excellent repeatability and uniformity in fabrication, and its low production cost. In actual calculations we made use of measured [21] etching rates in [100], [110], [111] and [311] crystal directions, for 30% KOH concentration at 70 °C (R_{111} = 0.005 μm/min, R_{100} = 0.797 μm/min, R_{110} = 1.455 μm/min and R_{311} = 1.436 μm/min). The actual shapes of the initial surfaces are described using simple geometrical abstractions. In the beginning of the calculations this descriptions are transformed into the initial level set functions using the fast marching method [14]. If the initial profile is defined with a bitmap mask, a special routine is used to generate corresponding initial level set function. Our implementation is based on ITK library [19]. The classes describing the level set function and the level set filter are reimplemented according to the procedures for treating non-convex Hamiltonians described in the previous section.

Since the cube is the simplest isometric crystal form [12], first we present the time evolution of the initial cube shape made of {100} planes. In Fig. 5, the changes of the cube form are shown at for equidistant time moments.

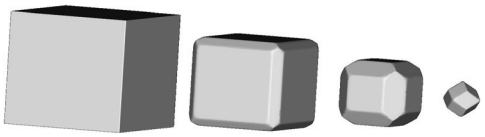

Fig. 5. Etching profiles of the silicon cube with initial edge of 50μm after 0s, 400s, 800s and 1200s, obtained using the four-parameter interpolation formula.

It is obvious that the initial cube shape gradually transforms to the final (rhombic) dodecahedron made of the fastest etching {110} principal planes, through the combinations of these shapes. It is expected given that dodecahedron is the only isometric form made of {110} planes. Almost the same results follow from the three and four parameters etching rates, given with relations (3) and (5) respectively, so we show only the later in Fig. 5. If the fastest planes are not {110} family, the final profile shape will change accordingly.

In order to test the strength of the method we have chosen to simulate etching of the silicon ball in KOH etchant. The initial spherical surface contains all possible velocity directions, so it is expected that the anisotropy of the etching process will produce the most dramatic changes of the initial shape. This shape, or more precisely hemisphere, is used in the experimental setup [21, 23] for measuring etching rates anisotropy, also. In such an experiment a hemisphere is only etched for a short time in order to minimize the inteference of neighbouring orientations. Here we shall follow etching process until its final stage.

Fig. 6 illustrates the changes of the initial spherical shape at four equidistant (reduced) time moments for both three and four parameters etching rates. In both cases the final stage is dodecahedron for the same reason as in the case of the cube shape. Of course, it

wouldn't be true, if the planes {110} are not the fastest. It is different from our preliminary results published in Ref. [24], where calculations with three parameters etching rates were performed on coarser mesh and with underestimated smoothing term in Lax–Friedrichs finite difference scheme. Intermediate shapes for the three and four parameters rates differ significantly.

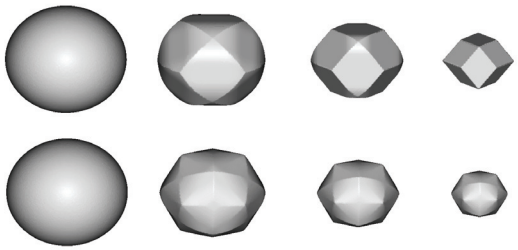

Fig. 6. Etching profiles of the sphere with initial radius of 25μm after 0s, 200s, 400s and 600s, obtained using (upper row) three- and (lower row) four-parameter interpolation formulas.

When high index directions <311> are not included (Fig. 6a) the transitional shape are composed of (quasi) tetrahexahedron, consisting of 24 triangles belonging to {012} family of planes, and dodecahedron crystal forms. Eventually the later prevails. By word "quasi" we mean curved, since the initial spherical shape cannot be transformed into polyhedral immediately. In the case when <311> directions are included and the angular dependence of the etching rates are given by (5), the evolution of the sphere begins with (quasi) hexoctahedron, the crystal form having 48 triangular faces belonging to {123} family of general planes.

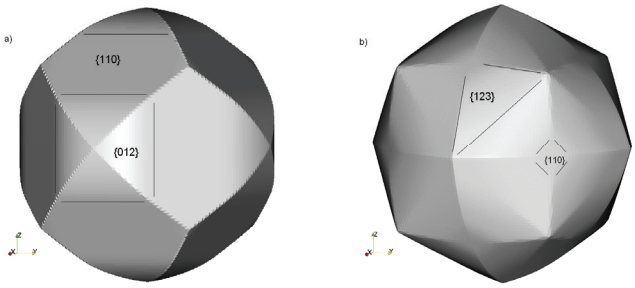

Fig. 7. An intermediate shape of the initial sphere obtained using a) three- and b) four-parameter interpolation formulas. The emerging crystal planes are denoted.

These intermediate shapes are displayed in Fig. 7, with some important geometrical elements denoted. Hexoctahedron is the form closest to the spherical shape, among all crystal forms. It is a very strong argument that the angular interpolation of the etching rate with four parameters is correct, and that it reproduces the most relevant aspects of silicon wet etching.

CONCLUSIONS

In this paper we have presented an application of the sparse field method for solving Hamilton-Jacobi equation with non-convex Hamiltonian in the 3D simulations of the profile surface evolution during anisotropic wet etching of silicon. It was shown that inclusion of additional directions for which the etching rates are known, would lead to the better quantitative agreement with the measured data. The resulting equations, describing interface surface evolution, are of Hamilton–Jacobi type and they can be solved using techniques developed for hyperbolic equations. The analysis of the obtained results confirm that regardless of the initial shape the profile evolution ends with the crystal form composed of the fastest etching planes, {110} in our model. Results presented here indicate that the sparse field level set method can be used as an effective tool for wet etching process modeling, and that it is a viable alternative to the cellular automata method, which is today widely used in for that purpose.

The present work has been carried out under MNZŽS 141025 project.

REFERENCES

1. M. Elwenspoek and H.V. Jansen, Silicon Micromachining, Cambridge University Press, 2004.
2. M.A. Gosalvez, Atomistic Modelling Of Anisotropic Etching Of Crystalline Silicon, PhD Thesis, Helsinki University of Technology, 2003.
3. Z. Zhu and C. Liu, Micromachining Process Simulation Using a Continuous Cellular Automata Method, J. Microelectromech. Syst., 9, 252-261 (2000).
4. Z. Zhou, Q. Huang, W. Li and W. Deng W, A cellular automaton-based simulator for silicon anisotropic etching processes considering high index planes, J. Micromech. Microeng. 17, S38-S49 (2007).
5. Z. Zhou, Q. Huang and W. Li, An atomic level model for silicon anisotropic etching processes - Cellular automaton simulation and experimental verification , Appl. Phys. Lett. 91, 174101 (2007).
6. M.A. Gosalvez, K. Sato, A.S. Foster, R.M. Nieminenn and H. Tanaka, An atomistic introduction to anisotropic etching , J. Micromech. Microeng. 17, S1-S26, (2007).
7. Y. Xing, M.A. Gosalvez and K. Sato, Step flow-based cellular automaton for the simulation of anisotropic etching of complex MEMS structures, New Journal of Physics 9, 436 (2007).
8. H. Schroder and E. Obermeier, A New Model for Si {100} Convex Corner Undercutting in Anisotropic KOH Etching, J. Micromech. Microeng. 10, 163-170 (2000).
9. T.J. Hubbard, MEMS Design - Geometry of silicon micromachining , Ph.D. Thesis, California Institute of Technology, 1994.
10. S. Osher and J.A. Sethian, Fronts Propagating with Curvature Dependent Speed: Algorithms Based on Hamilton-Jacobi Formulations, J. Comp. Phys. 79, 12-49 (1988).
11. J.A. Sethian, Evolution, Implementation, and Application of Level Set and Fast Marching Methods for Advancing Fronts, J. Comp. Phys. 169, 503-555 (2001).
12. J.A. Sethian and D. Adalsteinsson, An Overview of Level Set Method for Etching, Deposition and Lithography Development, IEEE Trans. Semiconductor Dev. 10, 167 (1996).
13. R. Whitaker, A Level-Set Approach to 3DReconstruction From Range Data, Int. J. Comp. Vision, 29, 203-231 (1998).
14. J. Sethian, Level Set Methods and Fast Marching Methods: Evolving Interfaces in Computational Fluid Mechanics, Computer Vision and Materials Sciences, Cambridge University Press, 1998.
15. S. Osher and R. Fedkiw, Level Set Method and Dynamic Implicit Surfaces, Springer-Verlag, New York, NY, 2002.
16. R. Tsai and S. Osher, Level Set Methods and Their Applications in Image Science, Comm. Math. Sci. 1, 623-656 (2003).
17. R. Fedkiw, G. Sapiro and C. Shu, Shock capturing, level sets, and PDE based methods in computer vision and image processing: a review of Osher's contributions, J. Comput. Phys. 185, 309-341 (2003).
18. L. Evans, Partial Differential Equation, American Mathematical Society, Providence, RI, 1998.
19. NLM Insight Segmentation and Registration Toolkit, Available: http://www.itk.org

20. B. Radjenović, J. K. Lee and M. Radmilović-Radjenović, Sparse field level set methodfor non-convex Hamiltonians in 3D plasma etching profile simulations ", Computer Physics Communications, 174, 127–132 (2006).
21. K. Sato, M. Shikida, Y. Matsushima, T. Yamashiro, K. Asaumi, Y. Iriye and M. Yamamoto, Characterization of orientation-dependent etching properties of single-crystal silicon - effects of KOH concentration, Sensors and Actuators A 64, 87-93 (1998).
22. M. Buerger, Elementary Crystalography, John Wiley & Sons, Inc., New York, Chapman & Hall, Limited, London, 1956.
23. M. Shikida, K. Sato, K. Tokoro and D. Uchikawa, Differences in anisotropic etchingproperties of KOH and TMAH solutions, Sensors and Actuators A 80, 179-188 (2000).
24. B. Radjenović, M. Radmilović-Radjenović and M. Mitrić, Non-convex Hamiltonians in 3D level set simulations of the wet etching of silicon, Appl. Phys. Lett. 89,213102 (2006)

PRIMENA LEVEL SET METODA NA NEKONVEKSNE HAMILTONIJANE

B. Radjenović, M. Radmilović-Radjenović, M. Mitrić

Primena level set metoda, proširenog na slučaj nekonveksnog Hamiltonijana, je ilustrovana rezultatima trodimenzionalne (3D) simulacije evolucije profila tokom anizotropnog hemijskog (mokrog) nagrizanja u silicijumu. Funkcije brzine nagrizanja su modelovane uzimajući u obzir svojstva simetrije silicijuma, korišćenjem interpolacione tehnike i eksperimentalno dobijenih vrednosti glavnih [100], [110], [111] i [311] pravaca u KOH rastvaraču. Rezultujuće level set jednačine su rešavane implementacijom sparse field metoda.